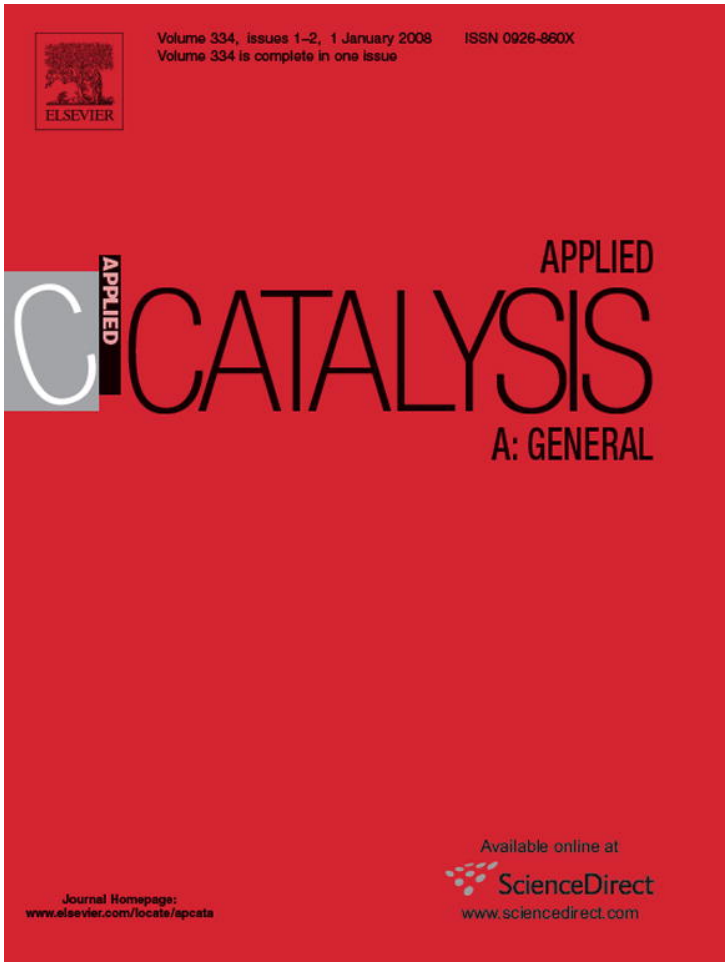

Available online at www.sciencedirect.com
ScienceDirect
Applied Catalysis A: General 334 (2008) 187–198
APPLIED CATALYSIS A: GENERAL
www.elsevier.com/locate/apcata

Effect of iron on the properties of sulfated zirconia

Amalia Luz Costa Pereira [a], Sergio Gustavo Marchetti [b], Alberto Albornoz [c], Patrício Reyes [d], Marcelo Oportus [d], Maria do Carmo Rangel [a,*]

[a] *Instituto de Química, Universidade Federal da Bahia, Campus Universitário de Ondina, 40170-290 Salvador, Bahia, Brazil*
[b] *CINDECA, Facultad de Ciencias Exactas, Universidad Nacional de La Plata, 1900, 47 y 115, La Plata, Argentina*
[c] *Centro de Química, Instituto Venezolano de Investigaciones Científicas, 21827 Caracas, Venezuela*
[d] *Facultad de Ciencias Químicas, Universidad de Concepción, Casilla 3-C, Concepción, Chile*

Received 27 May 2007; received in revised form 25 September 2007; accepted 29 September 2007
Available online 5 October 2007

Abstract

Sulfated zirconia has found several industrial applications, mainly for catalyzing reactions which require acidic sites. In order to control the properties of this solid, the effect of iron on the sulfated zirconia properties was studied in this work. Samples with different iron to zirconium molar ratios were prepared by the sol–gel method, followed by sulfation and characterization by several techniques. It was found that all iron ions go into zirconia when Fe/Zr $\leq$ 0.4. However, when higher amounts of iron (Fe/Zr $\geq$ 0.8) are added, hematite is segregated. Different phases can be obtained depending on the iron content and on the sulfur presence. Iron increases the specific surface areas of both sulfated and pure zirconia but does not affect the incorporation of sulfate groups as compared to pure zirconia. Iron also makes the solids thermally more stable and modifies the sulfated zirconia surface creating acidic sites with medium strength. Therefore, it is possible to control the acidity of the solid doping the sulfated zirconia with iron. All these changes are very useful for catalytic applications.

Keywords: Iron-doped zirconia; Sulfated iron oxide; Sulfated zirconia

1. Introduction

In the last few decades many investments have been done in the search for new catalysts that can fit the new requirements of the modern life. These materials should be able to be used in the petrochemical industry, as more efficient and versatile catalysts according to the new environmental laws, even more restrictive. As far as these features are concerned, the superacid solids are an attractive option, which could replace the liquid acids used as catalysts in the petrochemical industry. This substitution offers several advantages, such as the reduction of the production costs and of the environmental impact. The solid catalyst can be more easily separated from the products, allowing its regeneration and reutilization and thus decreasing the reactor corrosion and avoiding the discarding of acids in the environment. Therefore, the risk of handling great amounts of acid liquids is avoided [1].

Because of these advantages, a lot of papers dealing with the characteristics and properties of these solids aiming their use as catalysts have been published [2,3]. Among the superacid solids, sulfated zirconia is by far the most studied one, because of its potential for catalytic applications related to its acidity, higher than inorganic acids. It is well known that the characteristics and properties of sulfated zirconia depend on the conditions of the zirconium hydroxide preparation, the kind and concentration of sulfating agent, the impregnation time and the calcination temperature [4]. Due to the possibility of controlling these conditions, a considerable amount of papers have been published in the last years with the aim of tailoring the characteristics and properties of sulfated zirconia for specific applications [5,6].

Another way to control the properties of the sulfated inorganic oxides is the addition of other metals, producing mixed or doped systems. In particular, some metals can lead to more active catalysts and also more resistant against deactivation [7]. Therefore, several metals such as platinum, palladium, iridium, iron, tungsten, nickel, cobalt, chromium, titanium and manganese have been added to sulfated zirconia, producing

* Corresponding author. Tel.: +55 71 32836805; fax: +55 71 32355166.
E-mail address: mcarmov@ufba.br (M.d.C. Rangel).

0926-860X/$ – see front matter © 2007 Published by Elsevier B.V.
doi:10.1016/j.apcata.2007.09.042

more active and selective catalysts [8–10]. Among these modifying agents, platinum, iron and manganese have been identified as the most effective ones [7].

Previous works [11,12] have shown that the addition of manganese and iron oxide to sulfated zirconia increased in three orders of magnitude the catalytic activity during the *n*-butane isomerization. Other authors [9,13] have noted that these systems showed high activity in the conversion of propene to products such as hydrogen, paraffins, olefins and aromatics. A recent work in our laboratory [14] has shown that iron-doped sulfated zirconia catalysts are promising catalysts for toluene disproportionation to produce benzene and xylenes.

The present work intends to continue this study, through the preparation and characterization of sulfated zirconia samples, using less concentrated sulfuric acid during the sulfation process. The objective of this work is the development of an optimized preparation method, decreasing the handling and use of large amounts of sulfuric acid.

2. Experimental

2.1. Sample preparation

The samples were prepared by adding a zirconium oxychloride solution (1 mol L^{-1}) simultaneously with an ammonium hydroxide solution (25%), through a peristaltic pump, into a beaker with water. During the reagents addition the system was kept under stirring at room temperature. The final pH was adjusted to 10 using an ammonium hydroxide solution (25%). The sol produced was stirred for 24 h and then centrifuged (2000 rpm, 5 min). The gel obtained was washed with water and centrifuged again. These processes were repeated several times until no chloride ions were detected in the supernatant anymore. The gel was then dried in an oven at 393 K for 12 h. The solid thus obtained was ground and sieved in 100 mesh.

The sulfation process was performed by dispersing the zirconium hydroxide produced in a sulfuric acid solution (0.25 mol L^{-1}) and keeping the system for 30 min at room temperature. The system was then filtrated and the solid was dried for 12 h, at 393 K. The sulfated solid was calcined at 773 K for 4 h, under air flow (50 mL min^{-1}) at a rate of 10 K min^{-1} (Z25 sample). A reference system, without sulfation, was also prepared (Z sample) by this same procedure.

Three samples with different iron to zirconium molar ratio were produced: 0.2, 0.4 and 0.8. The solids were obtained by simultaneous hydrolysis of zirconium oxychloride and iron nitrate, using the ammonium hydroxide as precipitant agent by the same method described. The sulfated samples were named 2FZ25, 4FZ25 and 8FZ25 and the non-sulfated samples were named 2FZ, 4FZ and 8FZ, respectively, where FZ means zirconium doped with iron, the numbers on the left indicate the iron to zirconium molar ratio and the number on the right indicates the samples treated with a sulfuric acid solution (0.25 mol L^{-1}). Also, iron hydroxide was prepared through hydrolysis of iron nitrate with ammonium hydroxide, following the procedure described (F and F25 samples).

2.2. Catalyst characterization

The precursors (metal hydroxides) were analyzed by thermogravimetry (TG) to follow the effect of sulfation on the oxide formation. These analyses were carried out in a Metter Toledo model TGA/SDTA851 equipment, under air flow (50 mL min^{-1}), using a heating rate of 10 K min^{-1}, from room temperature up to 1273 K.

After the calcination, the samples were characterized by elemental chemical analysis, Fourier transform infrared spectroscopy (FTIR), X-ray diffraction (XRD), specific surface area measurements, temperature programmed reduction (TPR), acidity measurements by ammonia temperature programmed desorption (NH_3-TPD), X-ray photoelectron spectroscopy (XPS) and Mössbauer spectroscopy (MS).

The zirconium and iron analyses were performed by inductively coupled plasma atomic emission spectroscopy (ICP/AES) using an ARL model 3410 equipment. The sample (0.1 g) was previously dissolved using sulfuric acid and hydrochloric acid in a pump, for 2 h. The sulfur content in the samples was determined in an Leco model CS-200 equipment, using Lecocel and the iron chip accelerator.

The presence of sulfate groups in the samples was confirmed by FTIR, using a Perkin-Elmer model Spectrum One equipment, in the range of 400–4000 cm^{-1}. The samples were prepared as potassium bromide discs, in a 1:10 proportion. The XRD powder patterns of the solids were obtained in a Shimadzu model XD3A equipment, using Cu Kα ($\lambda = 0.15420$ nm) radiation and nickel filter, in a 2θ range between 10° and 80°, with a scanning speed of 2°/min.

The specific surface area measurements were carried out by the BET method in a Micromeritics model TPD/TPR 2900 equipment, using a 30% N_2/He mixture. The sample was previously heated at a rate of 10 K min^{-1} up to 443 K, under nitrogen flow (60 mL min^{-1}), remaining 30 min at this temperature. The TPR profiles were obtained in the same equipment. The samples (0.25–0.3 g) were reduced between 300 and 1273 K, at a rate of 10 K min^{-1}, using a 5% H_2/N_2 mixture.

The Micromeritics model TPD/TPR 2900 equipment was also used for the acidity measurements by NH_3-TPD. The sample was heated at 383 K, under nitrogen flow, during 30 min and then saturated with ammonia, injecting this gas through a calibrated loop. After cooling at room temperature, the temperature programmed desorption began, heating the solid from 303 up to 1043 K, under a heating rate of 10 K min^{-1}, using argon as gas carrier (45 mL min^{-1}).

The XPS spectra were acquired with a VG Scientific spectrometer, Escalab model 220i-XL, with source of X-rays, Mg Kα (1253 eV) anode and 4000 W power and hemispheric electron analyzer. This reference was in all cases in good agreement with the BE of the C 1s peak, arising from contamination, at 284.6 eV. This reference gives an accuracy of +0.1 eV.

The Mössbauer spectra at 298 and 25 K were taken in transmission geometry with a 512-channel constant acceleration spectrometer. A source of ^{57}Co in an Rh matrix of

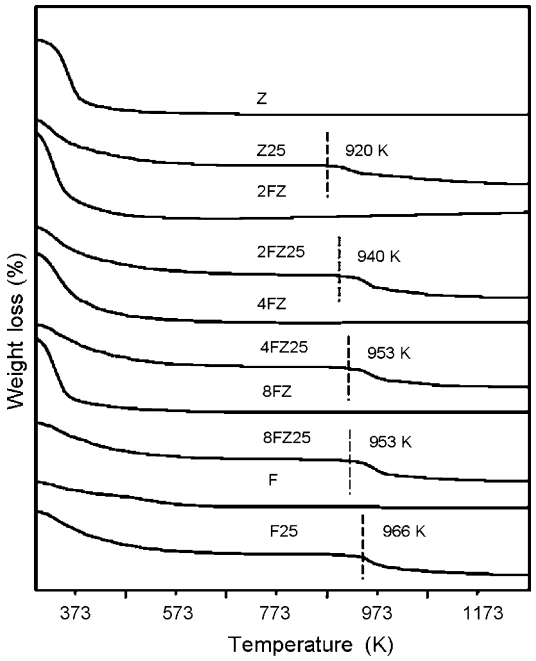

Fig. 1. Thermogravimetric curves for the metallic hydroxides.

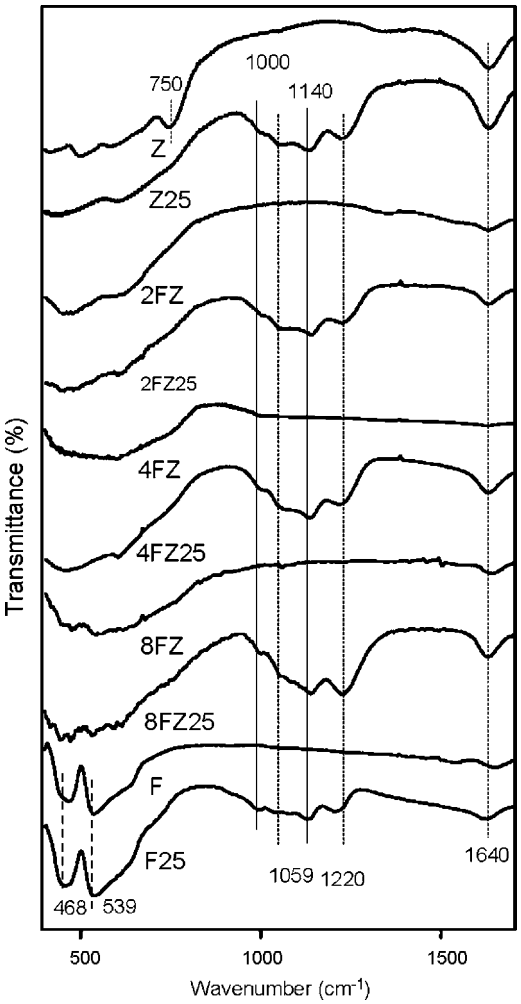

Fig. 2. FTIR spectra for the samples after calcination.

nominally 50 mCi was used. The velocity calibration was performed against a 12 μm-thick α-Fe foil. All isomer shifts (δ) mentioned in this paper are referred to this standard at room temperature. The temperature between 25 and 298 K was varied using a Displex DE-202 closed cycle cryogenic system. The spectra were folded to minimize geometric effects and were evaluated using a commercial computer fitting program named Recoil.

3. Results and discussion

Fig. 1 shows the thermogravimetric curves of the precursors. In the non-sulfated materials curves, it can be seen a weight loss in the range of 298–673 K, attributed to the loss of volatile materials and to zirconium and iron oxides formation [14,15]. On the other hand, the sulfated samples present weight loss in two stages, the first one between 298 and 673 K and the second one in the range of 873–1213 K. The weight loss at higher temperatures is attributed to sulfate groups decomposition. In the sulfated iron hydroxide, the sulfate groups decomposition began at about 966 K, while for the sulfated zirconium hydroxide the process was initiated at 920 K. In the sulfated zirconium–iron hydroxide samples, this process was initiated at intermediate temperatures (940–953 K), which are higher than the sulfated zirconium hydroxide. Fig. 1 shows the temperatures at which the decomposition of sulfate groups begins, calculated from the derivative curves. It can be seen that the temperature increased with the amount of iron in solids, except for the 8FZ25 sample. Therefore, the presence of iron in zirconia increased the stabilization of the sulfate groups and then they are more stable in iron-doped zirconia than in pure zirconia.

Table 1 shows the results of the chemical analysis of the solids after calcination. It is observed that the Fe/Zr molar ratios

Table 1
Chemical composition of the solids after calcination

Sample	Fe/Zr (molar) (±0.05)	% S (±0.03)	S/Zr (molar)	S/Fe (molar)	S/(Zr + Fe) (molar)
Z25	–	5.38	0.040	–	0.040
2FZ	0.19	–	–	–	–
2FZ25	0.18	6.24	0.050	0.72	0.047
4FZ	0.37	–	–	–	–
4FZ25	0.38	5.21	0.040	0.30	0.035
8FZ	0.80	–	–	–	–
8FZ25	0.75	5.21	0.050	0.18	0.039
F25	–	2.57	–	0.02	0.020

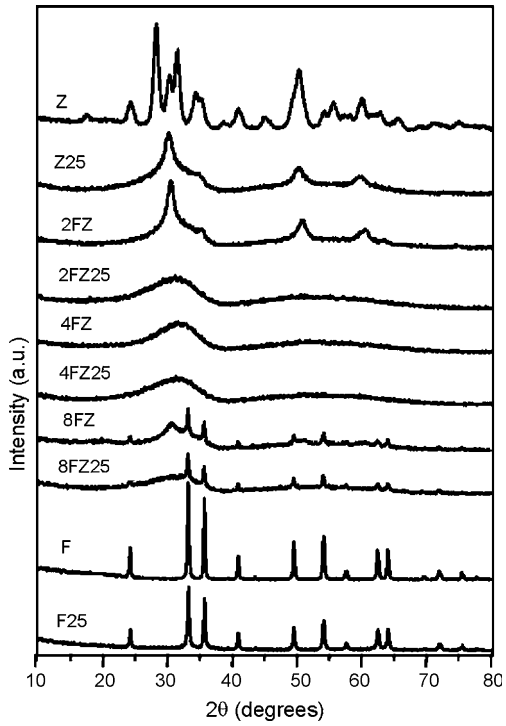

Fig. 3. X-ray diffractograms for the samples after calcination.

were close to the nominal values, indicating an appropriate precipitation of the iron and zirconium compounds. The sulfur content for sulfated zirconia was higher than for iron oxide, regardless the presence of iron. It means that zirconia is able to

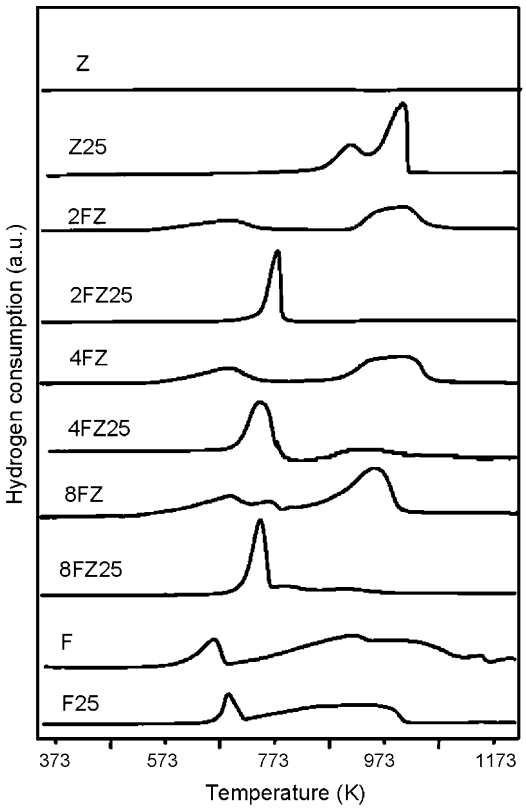

Fig. 4. TPR profiles for the calcined samples.

Table 2
Specific surface area (S_g) of the calcined solids

Sample	S_g (m^2/g)
Z	92
Z25	161
2FZ	216
2FZ25	223
4FZ	201
4FZ25	204
8FZ	176
8FZ25	148
F	20
F25	54

Table 3
Mössbauer spectra at 298 K of the sample 4FZ25 after the reduction at 1173 K

Species	Parameters	4FZ25
α-Fe^0	H (T)	32.9 ± 0.1
	δ (mm/s)	0.01 ± 0.01
	2ε (mm/s)	-0.03 ± 0.03
	%	32 ± 2
Fe_3O_4 sites A	H (T)	48.7 ± 0.7
	δ (mm/s)	0.27 ± 0.09
	2ε (mm/s)	0[a]
	%	6 ± 2
Fe_3O_4 sites B	H (T)	46.1 ± 0.5
	δ (mm/s)	0.77 ± 0.06
	2ε (mm/s)	0[a]
	%	10 ± 2
Fe^{2+} in cubic sites of FeO	δ (mm/s)	1.05 ± 0.01
	%	36 ± 2
Fe^{2+} in non-cubic sites of FeO	Δ (mm/s)	0.69 ± 0.05
	δ (mm/s)	0.93 ± 0.02
	%	16 ± 2

H: hyperfine magnetic field in Tesla; δ: isomer shift (all the isomer shifts are referred to α-Fe at 298 K); 2ε: quadrupole shift; Δ: quadrupole splitting.
[a] Parameters held fixed in fitting.

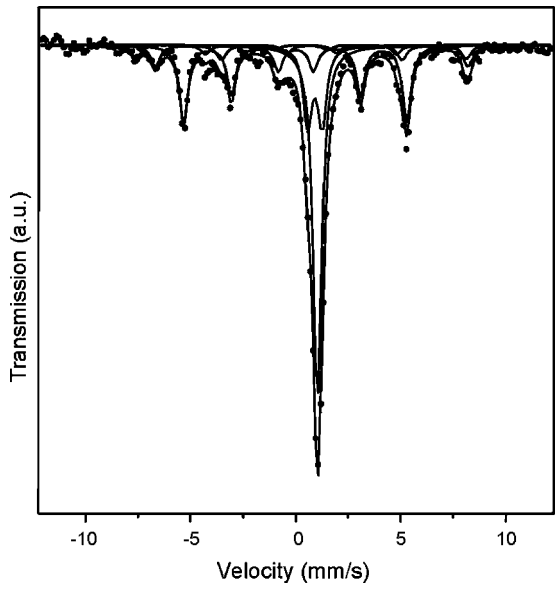

Fig. 5. Mössbauer spectra at 298 K for the 4FZ25 sample after the reduction at 1173 K.

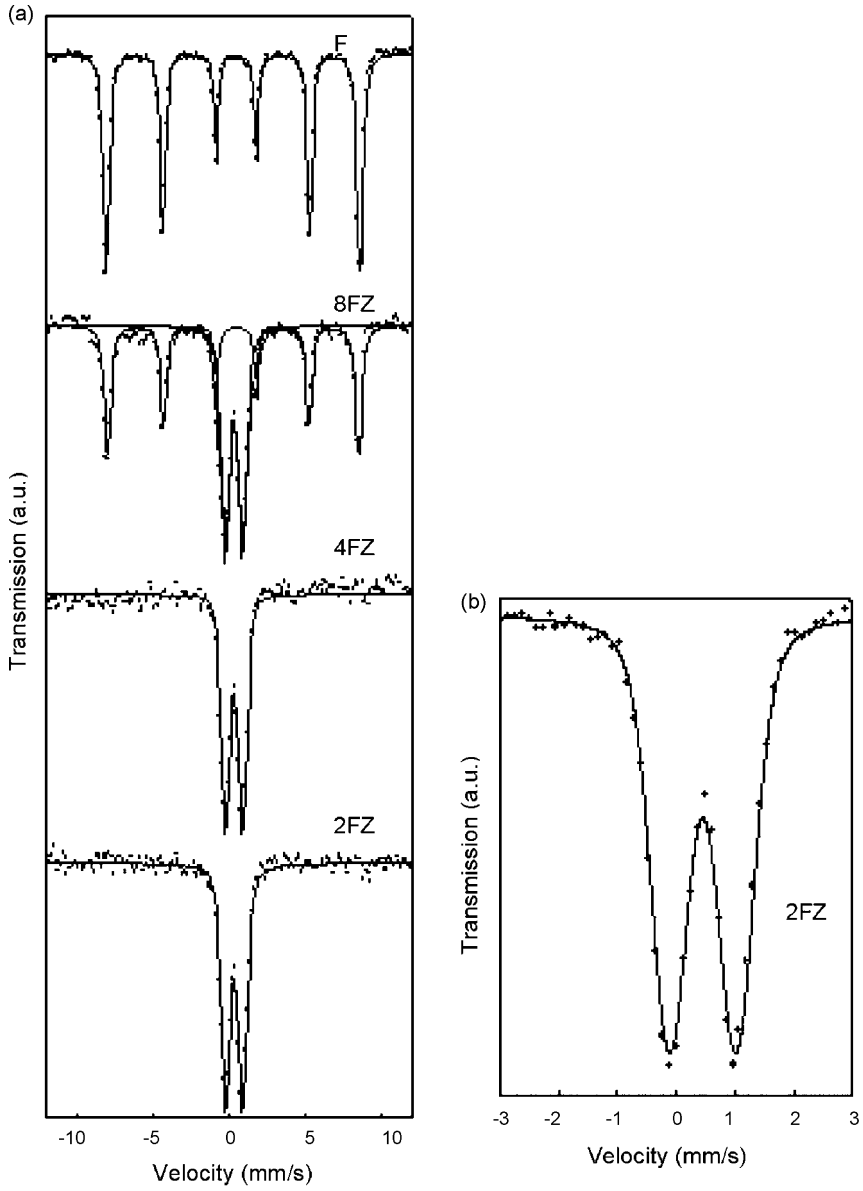

Fig. 6. (a) Mössbauer spectra at 298 K for the non-sulfated samples and (b) enlargement of the central area of the spectrum of the 2FZ sample.

accept more sulfate groups than iron oxide. However, these groups seem to be more stabilized in iron-containing samples than in zirconia, according to the results of thermogravimetry.

After calcination, the presence of sulfate groups was confirmed by FTIR spectroscopy, as shown in Fig. 2. It can be noted characteristic bands of the sulfate groups at 1000, 1059, 1140 and 1220 cm^{-1} [16,17]. Besides, a band at 1640 cm^{-1} is noticed, which is typical of the stretching and deformation vibrations of the water molecule [18]. The bands at 539 and 468 cm^{-1} are characteristics of the Fe–O bond vibrations and were observed for the iron oxide (F) and sulfated iron oxide (F25) samples [19]. In the zirconia spectrum it was also noted a band at 750 cm^{-1}, characteristic of Zr–O vibration [19]. For iron–zirconia samples, the band characteristics of the metal–oxygen bond could not be observed.

Fig. 3 shows the X-ray diffractograms of the calcined samples. Zirconia (Z) presents a typical profile of tetragonal and monoclinic phases, in agreement with previous works [20,21]. After sulfation (Z25) one can see broad and low intensity peaks, indicating the presence of a poorly crystallized solid and/or made off small particles, with the profile of the tetragonal phase of zirconia. This result is in agreement with previous studies [22], according to which the addition of sulfate groups to amorphous zirconium hydroxide promotes the stabilization of the tetragonal phase to the detriment of the monoclinic phase, which is more stable under this condition (773 K). These results are in accordance with our TG results, and also with previous works [21,23] which claim that sulfate samples should be calcined at temperatures around 823–873 K, if crystalline solids are desired.

The same behavior was noted for the 2FZ sample, indicating that iron is also able to stabilize the tetragonal phase of zirconia. This can be assigned to the presence of Fe^{3+} ions into the zirconia lattice, as confirmed by Mössbauer spectroscopy. This

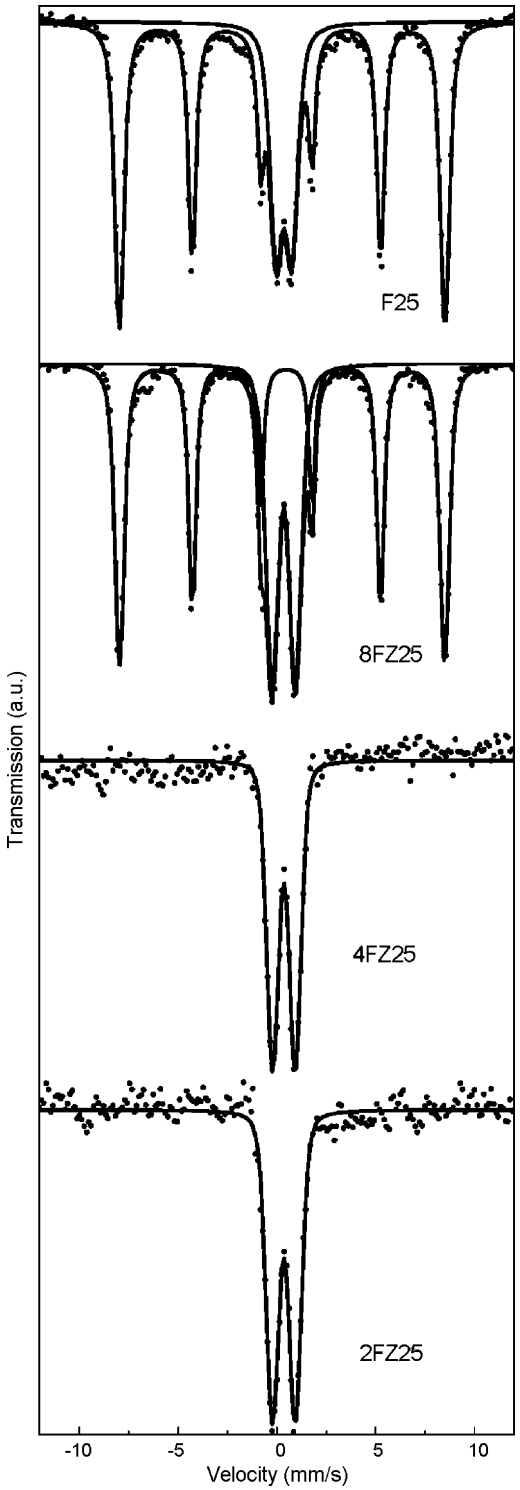

Fig. 7. Mössbauer spectra at 298 K for the sulfated samples.

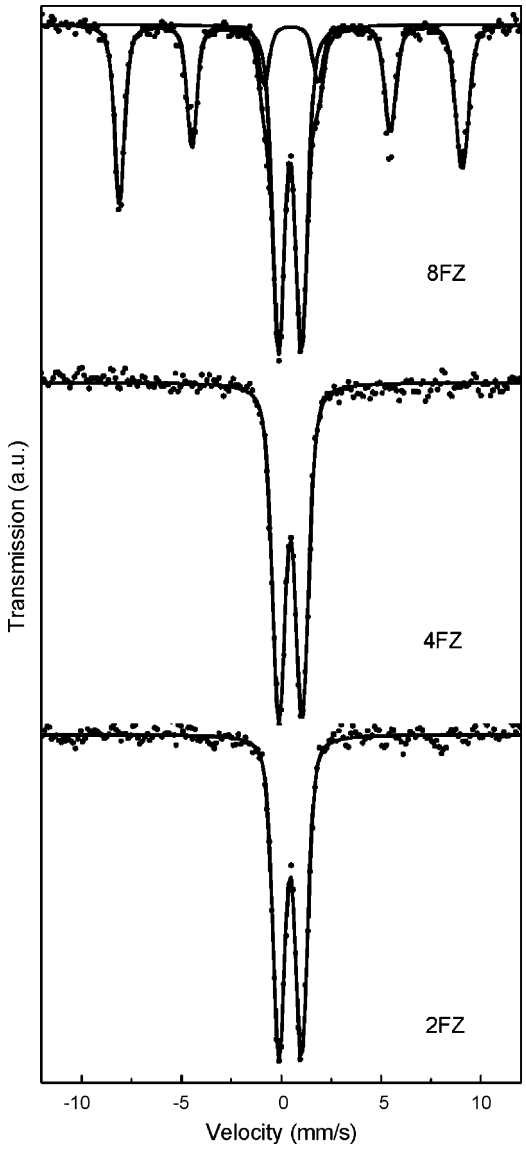

Fig. 8. Mössbauer spectra at 25 K for the non-sulfated samples.

stabilization also occurs with the addition of others ions, such as Eu^{3+}, Tb^{3+} and Sm^{3+}, into zirconia lattice, depending on the loading of the doping agent, as found by other authors [24]. However, this stabilization did not occur with the other samples, in accordance with these researchers who noted that this process depends on the amount of the dopant in solids. On the other hand, the solid with the highest iron loading (8FZ) showed peaks corresponding to hematite and also amorphous halos attributed to the zirconia tetragonal phase. The sample with the intermediate iron content (4FZ) showed only amorphous halos, indicative of a non-crystalline solid. After sulfation, the iron-containing samples showed the same profiles, indicating that this process did not change the kind and the degree of crystallinity of the phases. Characteristic peaks of hematite were produced by pure iron oxide (F), whereas sulfated iron oxide (F25) showed broader and lower intensity peaks, in agreement with literature [25].

The results of the specific surface area measurements of the solids are shown in Table 2. Regarding the pure oxides (Z25 and F25), the sulfate groups led to an increase in the specific surface area. Due to sulfation the zirconia specific surface area increased 75%, while an increment of 170% was showed by iron oxide. These results are in agreement with other works [25,26].

A significant increase of the specific surface area was obtained by addition of iron to zirconia. This effect did not

show dependence with the iron content and the differences are within the experimental error. Instead, the sulfated iron–zirconia samples did not experiment significant changes in the specific surface area as compared to iron-free samples.

Fig. 4 shows the TPR profiles of the samples. Zirconia (Z) was not reducible while iron oxide (F) showed two peaks around 673 and 873 K, assigned to the reduction of Fe^{3+} to Fe^{2+} and of Fe^{2+} to Fe^{0} species, respectively. The same processes were detected for the iron–zirconia samples. For these solids, the reduction seems to be more difficult: the maximum of the first peak was shifted to higher temperatures and the second peak began and finished at higher temperatures as compared to pure hematite.

The reduction profile of sulfated zirconia presented two peaks, attributed to the sulfate group reduction which produces SO_2, in agreement with other authors [23], who observed that this process occurs in the range from 673 to 973 K. The reduction peaks assignable to Fe^{3+} to Fe^{2+}, Fe^{2+} to Fe^{0} and sulfate groups to SO_2 were observed for sulfated iron oxide. However, sulfated iron–zirconia displayed just one peak that can be assigned to simultaneous reduction of sulfate and iron species. It can also be noted a shift of the reduction peak to lower temperatures in sulfated iron–zirconia as compared to sulfated zirconia. Therefore, it can be concluded that iron makes the sulfate groups reduction easier in zirconia. The presence of only one low temperature peak suggests that the Fe^{2+} species were stabilized in zirconia, during the reduction, making the metallic iron formation more difficult.

In order to verify if the Fe^{2+} species were stabilized in zirconia during the TPR experiments, a Mössbauer spectrum was taken on the 4FZ25 sample after the reduction at 1173 K, in the same condition. The results are shown in Fig. 5 and Table 3. The spectrum was fitted with three sextuplets, one doublet and one singlet. The sextuplets with higher hyperfine magnetic fields correspond to magnetite [27], while the remaining one belongs to α-Fe^{0}. On the other hand, the singlet and the doublet can be assigned to wustite (FeO), fitted by the methodology proposed by McCammon and Price [28], who used a singlet for identifying the Fe^{2+} species in a cubic environment (Fe_A^{2+}) in $Fe_{0.981}O$. This site is identical to that for stoichiometric FeO. They also used two doublets for iron ions in a non-cubic environment (Fe_B^{2+} and Fe_C^{2+}). In the present work, the site related to Fe_B^{2+} result in the fitting and only the singlet and the doublet remained. Therefore, there are 52% of FeO, 32% of α-Fe^{0} and 16% of Fe_3O_4 in the sample.

The Mössbauer spectra obtained for non-sulfated and sulfated samples at 298 and 25 K are displayed in Figs. 6–9 and their hyperfine parameters – obtained from the fittings – are shown in Tables 4–7. The parameters of F sample are typical of α-Fe_2O_3 [29] which are in agreement with the XRD result. In comparison with this sample, the sulfated iron oxide one (F25) presented a crystal size diminution. This was inferred by the appearance of a superparamagnetic α-Fe_2O_3 signal, represented by a doublet at room temperature, which is magnetically blocked at 25 K. This signal was attributed to very small particles or to the presence of surface Fe^{3+} species, since its quadrupole shift was about 0 mm/s and the magnetic hyperfine field was significantly decreased [30]. This behavior can be explained assuming that sulfuric acid can caused a dissolution-recrystallization process, producing very small particles. This result explains the specific surface area increase due to sulfation and the XRD broadening peaks in F25.

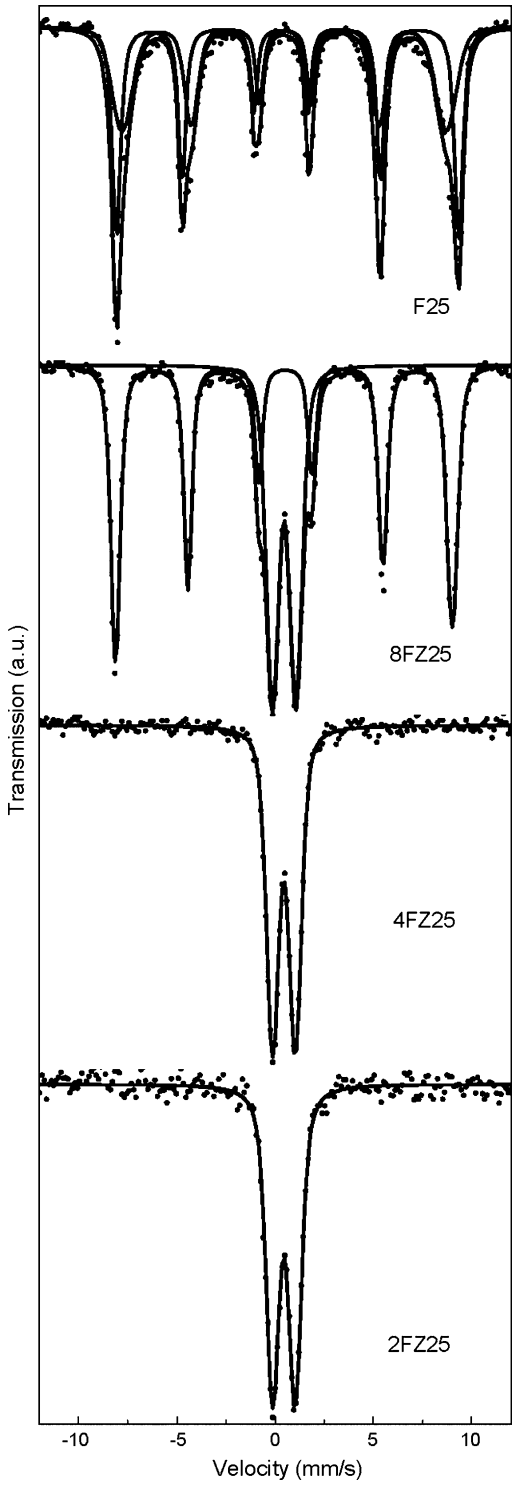

Fig. 9. Mössbauer spectra at 25 K for the sulfated samples.

The 8FZ Mössbauer spectra at 298 and 25 K presented two signals, one sextuplet and one doublet. The sextuplet can be

Table 4
Mössbauer parameters of non-sulfated samples at 298 K

Species	Parameters	F	8FZ	4FZ	2FZ
α-Fe_2O_3	H (T)	51.6 ± 0.1	–	–	–
	δ (mm/s)	0.37 ± 0.01	–	–	–
	2ε (mm/s)	-0.22 ± 0.01	–	–	–
	%	100	–	–	–
α-Fe_2O_3 with Zr^{4+}	H (T)	–	51.1 ± 0.1	–	–
	δ (mm/s)	–	0.37 ± 0.01	–	–
	2ε (mm/s)	–	-0.22 ± 0.01	–	–
	%	–	51 ± 1	–	–
Fe^{3+} in ZrO_2	Δ	–	1.11 ± 0.01	1.12 ± 0.02	1.10 ± 0.01
	δ	–	0.33 ± 0.01	0.34 ± 0.01	0.34 ± 0.01
	%	–	49 ± 1	100	100

H: hyperfine magnetic field in Tesla; δ: isomer shift (all the isomer shifts are referred to α-Fe at 298 K); 2ε: quadrupole shift; Δ: quadrupole splitting.

Table 5
Mössbauer parameters of sulfated samples at 298 K

Species	Parameters	F25	8FZ25	4FZ25	2FZ25
α-Fe_2O_3	H (T)	51.0 ± 0.1	–	–	–
	δ (mm/s)	0.37 ± 0.01	–	–	–
	2ε (mm/s)	-0.22 ± 0.01	–	–	–
	%	70 ± 1	–	–	–
Superparamagnetic α-Fe_2O_3	Δ	0.78 ± 0.01			
	δ	0.35 ± 0.01			
	%	30 ± 1			
α-Fe_2O_3 with Zr^{4+}	H (T)	–	50.9 ± 0.1	–	–
	δ (mm/s)	–	0.37 ± 0.01	–	–
	2ε (mm/s)	–	-0.22 ± 0.01	–	–
	%	–	61 ± 1	–	–
Fe^{3+} in ZrO_2	Δ	–	1.18 ± 0.01	1.15 ± 0.02	1.15 ± 0.02
	δ	–	0.34 ± 0.01	0.35 ± 0.01	0.35 ± 0.02
	%	–	39 ± 1	100	100

H: hyperfine magnetic field in Tesla; δ: isomer shift (all the isomer shifts are referred to α-Fe at 298 K); 2ε: quadrupole shift; Δ: quadrupole splitting.

attributed to hematite, with Fe^{3+} ions isomorphically substituted by Zr^{4+}. This can be deduced considering that the magnetic hyperfine field was decreased as compared to pure hematite at both temperatures, the Morin transition did not occur at 25 K and at this temperature an important magnetic hyperfine fields distribution appeared, correlated with the isomer shift. It would indicate a change in the Fe^{3+} environments, produced by the presence of different Zr^{4+} neighbors numbers. This result is in agreement with Stefanic et al. [31]. On the other hand, the doublet detected at 298 K could be assigned to superparamagnetic hematite, but this assumption can be discarded, considering the followings reasons: the doublet has a very large quadrupole splitting – higher than for superparamagnetic α-Fe_2O_3 – and the percentage of the both signals appear unchanged at 25 K. If superparamagnetic α-Fe_2O_3 would be present, the percentage of the magnetic signal would increases and the percentage of the doublet would decreases when the temperature decreases. Therefore, we can conclude that the doublet signal is produce by paramagnetic Fe^{3+} ions. In some situations the α-Fe_2O_3

Table 6
Mössbauer parameters of non-sulfated samples at 25 K

Species	Parameters	8FZ	4FZ	2FZ
α-Fe_2O_3 with Zr^{4+}	H (T)	53.2 ± 0.1	–	–
	δ (mm/s)	0.49 ± 0.01	–	–
	2ε (mm/s)	0.01 ± 0.02	–	–
	%	50 ± 1	–	–
Fe^{3+} in ZrO_2	Δ	1.15 ± 0.01	1.17 ± 0.01	1.14 ± 0.02
	δ	0.44 ± 0.01	0.46 ± 0.01	0.45 ± 0.01
	%	50 ± 1	100	100

H: hyperfine magnetic field in Tesla; δ: isomer shift (all the isomer shifts are referred to α-Fe at 298 K); 2ε: quadrupole shift; Δ: quadrupole splitting.

Table 7
Mössbauer parameters of sulfated samples at 25 K

Species	Parameters	F25	8FZ25	4FZ25	2FZ25
α-Fe_2O_3	H (T)	54.0 ± 0.1	–	–	–
	δ (mm/s)	0.47 ± 0.01	–	–	–
	2ε (mm/s)	0.33 ± 0.01	–	–	–
	%	50 ± 2	–	–	–
α-Fe_2O_3 very small particles	H (T)	51.1 ± 0.2	–	–	–
	δ (mm/s)	0.48 ± 0.01	–	–	–
	2ε (mm/s)	-0.05 ± 0.02	–	–	–
	%	50 ± 2	–	–	–
α-Fe_2O_3 with Zr^{4+}	H (T)	–	53.1 ± 0.1	–	–
	δ (mm/s)	–	0.49 ± 0.01	–	–
	2ε (mm/s)	–	-0.07 ± 0.01	–	–
	%	–	59 ± 1	–	–
Fe^{3+} in ZrO_2	Δ	–	1.19 ± 0.01	1.15 ± 0.01	1.15 ± 0.02
	δ	–	0.46 ± 0.01	0.45 ± 0.01	0.45 ± 0.01
	%	–	41 ± 1	100	100

H: hyperfine magnetic field in Tesla; δ: isomer shift (all the isomer shifts are referred to α-Fe at 298 K); 2ε: quadrupole shift; Δ: quadrupole splitting.

particle sizes are extremely small to get a total magnetic blocking of the magnetization vector at 25 K. Nevertheless, still in these cases the onset of the blocking is detected at 25 K since the background of the spectrum appears curved. The present spectrum did not show a curved background. These paramagnetic ions can be assigned to Fe^{3+} cations located into the zirconium lattice. The assignment of this signal is in agreement with Stefanic et al. [31,32]. The 4FZ and 2FZ samples showed only one doublet at both temperatures assignable, in the same way that 8FZ, to Fe^{3+} into zirconium oxide lattice also.

The spectra of iron–zirconia samples remained unchanged after the sulfation process. Iron sulfate was not detected in any sample.

As expected, sulfation caused an important increase in the acidity in solids, as we can see in Table 8. All the sulfated solids presented greater number of acidic sites than the respective reference samples. Besides, the iron addition also caused an increase of the number of acidic sites for the non-sulfated solids and this effect decreased with the increase of the Fe/Zr molar ratio.

The sulfated iron–zirconia solids presented a less number of acidic sites than the sulfated zirconia, except the material with low iron loading (2FZ25). However, when the number of ammonia molecules is compared per solid area, the materials doped with iron present approximately the same density of acidic sites as the sulfated zirconia. On the other hand, the iron oxide showed a higher density of acidic sites, a fact which can be assigned to the higher amount of sulfate groups on its surface, as shown by the XPS results (Table 10).

The NH_3-TPD profiles are presented in Fig. 5. Although ammonia TPD is not the most suitable technique for

Table 8
Acidity (expressed as number of desorbed ammonia molecules) of the calcined solids

Sample	Molecules NH_3 ($\times 10^{-19}$ g^{-1})	Molecules NH_3 ($\times 10^{-17}$ m^{-2})
Z	1.62	1.76
Z25	7.40	4.60
2FZ	3.76	1.74
2FZ25	9.93	4.45
4FZ	3.56	1.77
4FZ25	7.22	3.54
8FZ	3.34	1.89
8FZ25	6.14	4.15
F	0.45	2.25
F25	4.94	9.15

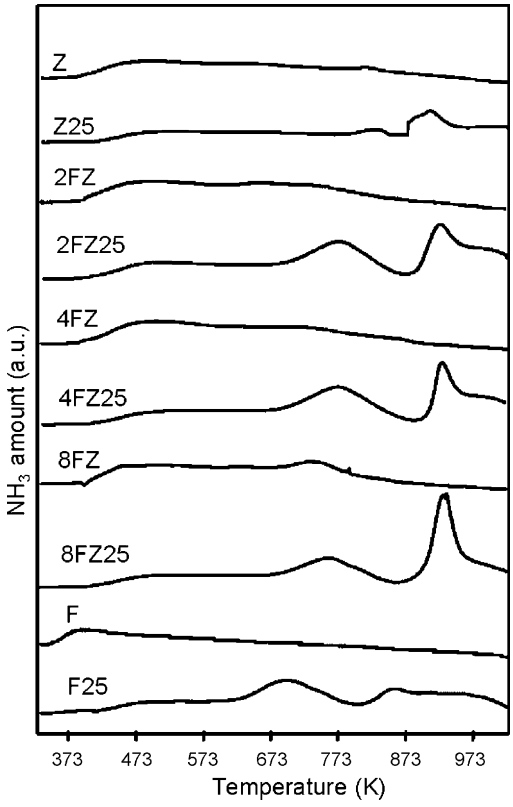

Fig. 10. NH_3-TPD profiles for the calcined samples.

Table 9
Surface elemental composition of the calcined samples

Sample	Fe/Zr (molar)	S/Fe (molar)	S/Zr (molar)	S/(Zr + Fe) (molar)
Z25	–	–	0.11	0.11
2FZ	0.11	–	–	–
2FZ25	0.05	5.34	0.25	0.24
4FZ	0.11	–	–	–
4FZ25	0.10	1.63	0.16	0.14
8FZ	0.08	–	–	–
8FZ25	0.24	2.27	0.54	0.43
F25	–	0.99	–	0.99

determining acidity in sulfate samples, since ammonia decomposes sulfate at high temperatures, it is acceptable for qualitative investigation of the strength of the acid sites [33]. From Fig. 10, it can be noted that the non-sulfated zirconia showed a broad low temperature peak, which is extended in a wide range of temperature and corresponds to sites of weak and medium strength, in accordance with previous work [21,34] and can be assigned to ammonia adsorbed on weak Lewis sites [21]. The other non-sulfated solids showed similar profiles, showing that the addition of iron did not increase the strength of the acidic sites. On the other hand, the sulfated samples present curves with two intense desorption peaks, assignable to medium and strong acidic strength sites [34], although the high temperature peak may include also the partial decomposition of the sulfate groups. It can be noted that the addition of iron to sulfated zirconia (Z25) creates sites of medium strength as can be inferred by a broad peak in the range of 673–873 K for the 2FZ25, 4FZ25 and 8FZ25 samples.

It also can be noted, from Table 9, that the surface S/(Zr + Fe) ratios did not present a regular variation with the iron content in the solids. In all cases, the surface Fe/Zr molar ratio was lower than in the bulk (Table 1). Besides, this ratio was not affected by the iron loading for the non-sulfated solids, indicating that for the 4FZ and 8FZ samples most of iron went to the bulk and just a limited amount remained on the surface. On the other hand, the surface Fe/Zr ratio was increased with the total iron loading for the sulfated samples. In spite of this fact, if we compare the Fe/Zr ratio in the bulk (Table 1) and on the surface (Table 9), for the 4FZ25 and 8FZ25 samples, we can see that most of iron is inside the solid also, mainly in the last case. It suggests that hematite, detected by X-ray diffraction in this sample, is mainly occluded in the solid and does not contribute to increase the stability of sulfate groups. Therefore, one can suppose that these groups were more stable in 4FZ25 sample than in 2FZ25 because more iron was incorporated in zirconia lattice; however in the 8FZ25 sample the stability did not change, as compared to the 4FZ25 one, probably because the lattice was not able to accept iron anymore and then it segregates as hematite. These findings can explain our TG results.

The binding energies (BE) of some characteristic core levels of zirconium, iron, sulfur and oxygen in the samples are displayed in Table 10. The binding energies for the Zr $3d_{5/2}$ and Zr $3d_{3/2}$ peaks are in close agreement with those for Zr^{4+} in ZrO_2-type compounds [35] and in accordance with previous work [36]. In the sulfated samples, the peaks are broader as shown in Fig. 11, but no significant difference was found among the binding energies. For pure iron oxide the spectrum showed a doublet, with the main peak ($2p_{3/2}$) at around 709.5 eV (Table 10 and Fig. 12), which are typical of Fe^{3+} species [35].

Table 10
Binding energies (eV) of the samples after calcination

Sample	Binding energy (eV)				
	Zr $3d_{3/2}$	Zr $3d_{5/2}$	Fe $2p_{3/2}$	O 1s	S 2p
Z	184.2	181.8		527.8 530.5	
Z25	184.9	182.5		527.8 530.5 532.3	169.1
2FZ	184.2	181.1	710.2	527.5 529.8	
2FZ25	184.5	182.1	710.5	527.4 530.0 532.1	168.1
4FZ	184.0	181.6	710.5	527.8 529.6	
4FZ25	184.4	182.0	709.7	526.5 529.9 531.9	168.5
8FZ	183.8	181.4	709.9	527.3 529.4	
8FZ25	184.4	182.0	710.1	528.2 529.9 531.8	167.07
F			709.5	526.9 529.5	
F25			709.9	527.6 529.9 531.8	167.4

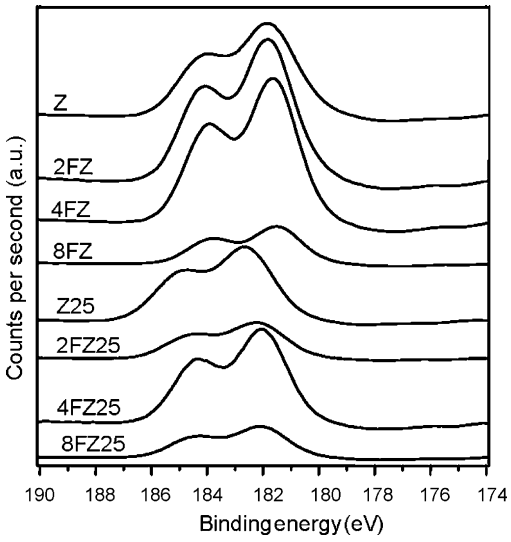

Fig. 11. Zr 3d core-level spectra for the samples.

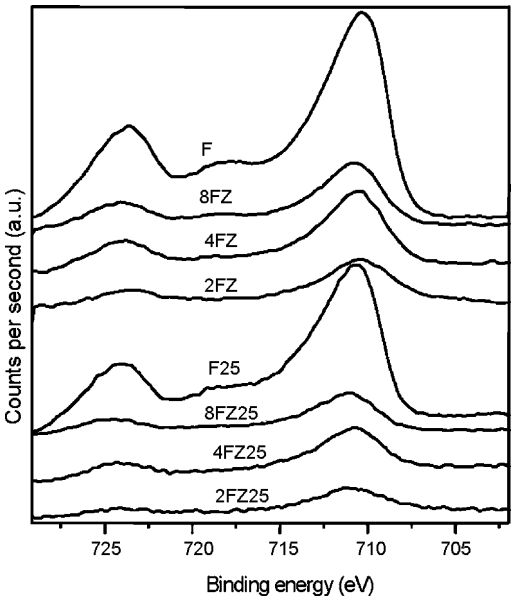

Fig. 12. Fe 2p core-level spectra for the samples.

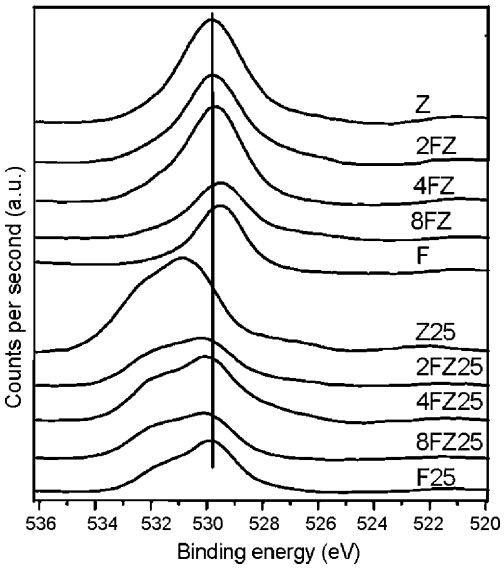

Fig. 14. O 1s core-level spectra for the samples.

The presence of sulfur in the samples was detected by the binding energy at around 169.1 eV in agreement with sulfur in sulfates [35] and with previous results regarding sulfate samples [37]. The S 2p spectra are similar for all the samples and show no peculiarities, as displayed in Fig. 13. The zirconia-based samples showed an additional peak at higher energy, due to the satellite peak of Zr 3d. It can be noted that the presence of iron shifted the peak to lower values of binding energy; for the 8FZ25 sample this value is close to that of pure hematite, in accordance to the high amount of iron in this sample.

Fig. 14 shows the O 1s spectra for the samples. For the non-sulfated samples, the fitting has been performed by two components, the main at lower energy assigned to oxygen in the oxide lattice and the second related to the surface OH groups [35,36]. For the sulfated samples, the spectra become broader and were fitted by three components. The lower and the second peaks are due to oxygen in the oxide and to the surface OH groups, respectively while the higher energy component (around 532.0 eV) is related to oxygen in sulfates [35,36,38].

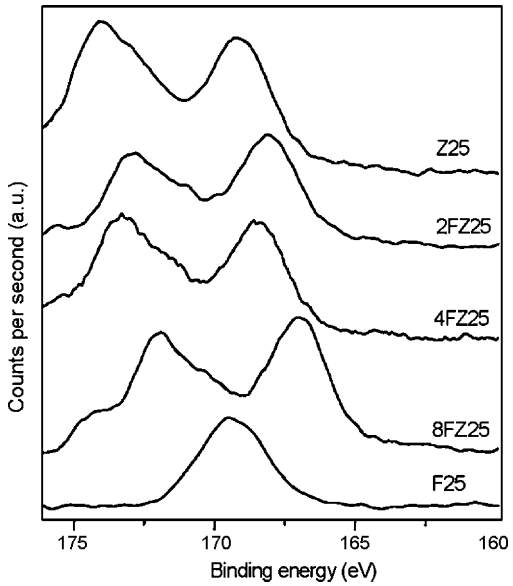

Fig. 13. S 2p core-level spectra for the samples.

4. Conclusions

The effect of iron on the sulfated zirconia properties was studied in this work. It was observed that there is an iron concentration range ($Fe/Zr \leq 0.4$), where the entire metal amount is incorporated into zirconia. The addition of higher amounts of iron ($Fe/Zr \geq 0.8$) produces the segregation of hematite. The iron presence did not affect the incorporation of sulfate groups by sulfation and these groups are thermally more stable, as compared to pure zirconia. The solid with lower iron loading has a larger amount of acidic sites, 34% more than pure sulfated zirconia.

Iron modifies the sulfated zirconia surface, generating acidic sites of medium strength. This means that doping adequately the sulfated zirconia with iron it is possible to get two effects: increase the total number of acidic sites and generate a new type of acidic sites with lower strength. These changes, especially the simultaneous presence of two acidic type sites with different strengths, are interesting for several catalytic applications.

Acknowledgements

ALCP acknowledges FAPESB for her graduate fellowship. The authors thank FAPESB and FINEP for the financial support.

References

[1] M. Golombok, J. Brujin, Appl. Catal. A 208 (2001) 47.
[2] V.M. Benítez, R. Carlos, C.L. Vera, F.G. Pieck, J.C. Lacamoire, J. Yori, M. Grau, J.M. Parera, Catal. Today 107 (2005) 651.

[3] B.M. Reddy, P.M. Sreekanth, P. Lakshmanan, J. Mol. Catal. A 237 (2005) 93.
[4] J.R. Sohn, H.W. Kim, J. Mol. Catal. 52 (1989) 361.
[5] B.M. Reddy, P.M. Sreekanth, P. Lakshmanan, A. Khan, J. Mol. Catal. A 244 (2006) 1.
[6] B.M. Reddy, P.M. Sreekanth, Y. Yamada, T. Kobayashi, J. Mol. Catal. A 227 (2005) 81.
[7] G.D. Yadav, J.J. Nair, Micropor. Mesopor. Mater. 33 (1999) 1.
[8] F. Lónyi, J. Valyon, J. Engelhradt, F. Mizukami, J. Catal. 160 (1996) 279.
[9] T. Cheung, F.C. Lange, B.C. Gates, J. Catal. 159 (1996) 99.
[10] K.T. Wan, C.B. Khouw, M.E. Davis, J. Catal. 158 (1996) 311.
[11] C.Y. Hsu, C.R. Heimbuch, C.T. Armes, B.C. Gates, J. Chem. Soc., Chem. Commun. (1992) 1645.
[12] V. Adeeva, G.D. Lei, W.M.H. Sachtler, Appl. Catal. A 118 (1994) L11.
[13] R. Rudham, A.W. Winstanley, J. Chem. Soc., Faraday Trans. 91 (1995) 1689.
[14] A.L.C. Pereira, P.S.S. Nobre, A. Albornoz, P. Reyes, M. Oportus, M.C. Rangel, Anais do XX SICAT—Simpósio Ibero-Americano de Catálise, Gramado, RS, Brazil, 2006.
[15] G. Magnacca, G. Cerrato, C. Morterra, M. Signoretto, F. Somma, F. Pinna, Chem. Mater. 15 (2003) 675.
[16] T. Yamaguchi, Appl. Catal. A 61 (1990) 1.
[17] K. Arata, Adv. Catal. 37 (1990) 165.
[18] B. Stuart, B. George, P. McIntryre, Modern Infrared Spectroscopy, John Wiley & Sons Ltd., England, 1996.
[19] S.H. Yariv, E. Mendelovici, Appl. Spectrosc. 33 (1979) 410.
[20] J.C. Duchet, M.J. Tilliete, D. Cornet, Catal. Today 10 (1991) 507.
[21] W.-H. Chen, H.-H. Ko, A. Sakthivel, S.-J. Huang, S.-H. Liu, A.-Y. Lo, T.-C. Tsai, S.-B. Liu, Catal. Today 116 (2006) 111.
[22] R.A. Comelli, C.R. Vera, J.M. Parera, Latin Am. Appl. Res. 24 (1994) 227.
[23] J.M. Grau, J.C. Yori, J.M. Parera, Appl. Catal. 1 (1981) 367.
[24] W. Córdova-Martínez, E. De la Rosa-Cruz, L.A. Díaz-Torres, P. Sales, A. Montoya, M. Avendaño, R.A. Rodríguez, O. Barbosa-García, Opt. Mater. 20 (2002) 263.
[25] A.S.C. Brown, J.S.J. Hargreaves, B. Rijniersce, Catal. Today 45 (1998) 47.
[26] D.A. Ward, E.I. Ko, J. Catal. 150 (1994) 18.
[27] R.E. Vandenberghe, E. De Grave, in: G.J. Long, F. Grandjean (Eds.), Mössbauer Spectroscopy Applied to Inorganic Chemistry, Plenum Press, New York, 1989 , p. 59 (Chapter 3).
[28] C.A. McCammon, D.C. Price, Phys. Chem. Miner. 11 (1985) 250.
[29] E. Murad, J.H. Johnston, in: G.J. Long (Ed.), Mössbauer Spectroscopy Applied to Inorganic Chemistry, vol. 2, Plenum Publishing Corporation, 1987.
[30] M. Vazquez Mansilla, R.D. Zysler, C. Arciprete, M.I. Dimitrijewits, C. Saragovi, J.M. Greneche, J. Magn. Magn. Mater. 204 (1999) 29.
[31] G. Stefanic, B. Grzeta, K. Nomura, R. Trojko, S. Music, J. Alloys Compd. 327 (2001) 151.
[32] G. Stefanic, S. Music, S. Popovic, K. Nomura, J. Mol. Struct. 481 (1999) 627.
[33] K. Föttinger, K. Zorn, H. Vinek, Appl. Catal. A: Gen. 284 (2005) 69.
[34] J.C. Yori, J.C. Luy, J.M. Parera, Catal. Today 5 (1989) 493.
[35] C.D. Wagner, W.N. Rigns, L.E. Davis, J.F. Moulder, Handbook of X-ray Photoelectron Spectroscopy, Perkin-Elmer, Eden Praire, 1992.
[36] S. Ardizone, C.L. Bianch, E. Grassi, Colloids Surf. 135 (1998) 41.
[37] S. Ardizone, C.L. Bianch, E. Grassi, Appl. Surf. Sci. 152 (1999) 63.
[38] V. Inodovina, M.C. Campa, D. Pietrogiaconi, Surf. Sci. Catal. 130 (2000) 1439.